Maximizing Target Detection under Sunlight Reflection on Water Surfaces with an Autonomous Unmanned Aerial Vehicle

Hyukseong Kwon[1], Josiah Yoder[1], Stanley Baek[1], Scott Gruber[1], and Daniel Pack[2]

Abstract— Reflected sunlight can significantly impact vision-based object detection and tracking algorithms, especially ones based on an aerial platform operating over a marine environment. Unmanned aerial systems above a water surface may be unable to detect objects on the water surface due to sunlight glitter. Although the area affected by sunlight reflection may be limited, rapid course corrections of unmanned aerial vehicles (UAVs) – especially fixed-wing UAVs – is also limited by aerodynamics, making it challenging to determine a reasonable path that avoids sunlight reflection while maximizing chances to capture a target. In this paper, we propose an approach for autonomous UAV path planning that maximizes the accuracy of the estimated target location by minimizing the sunlight reflection influences.

I. INTRODUCTION

Autonomous target detection and tracking are two of the most critical capabilities required of unmanned aerial vehicles (UAVs) as they provide fundamental building-blocks for higher-level algorithms such as target identification, behavior recognition, and target geolocation, among many others. In a marine environment, one of the major challenges to target detection and tracking is the presence of sunlight (or other light sources) reflected on the water surface, making target detection/tracking much more problematic. Not only does reflected sunlight distract target detection, the reflected light can distort the target's visual information or wash it out completely. Figure 1 is a sample image presenting sunlight reflection on water surfaces.

In order to predict where sunlight reflection occurs, we use a *bidirectional reflection distribution function* (BRDF) [1]. The BRDF is a model to estimate reflected radiance using four different elements: azimuth and elevation angles of an incident light ray, and azimuth and elevation angles of an outgoing light ray. In the case of sunlight, the azimuth and elevation of the incident light can be predetermined based upon location, date, and time of day. However, given the roughness of the ocean surface, the outgoing light will be scattered in many directions. The BRDF allows us to compute the strength of the reflected light in any of these directions.

Well-accepted BRDF models for light reflection include the *Torrance-Sparrow* model [2], the *Phong* reflectance model [3], and the *Oren-Nayar* model [4]. Torrance and
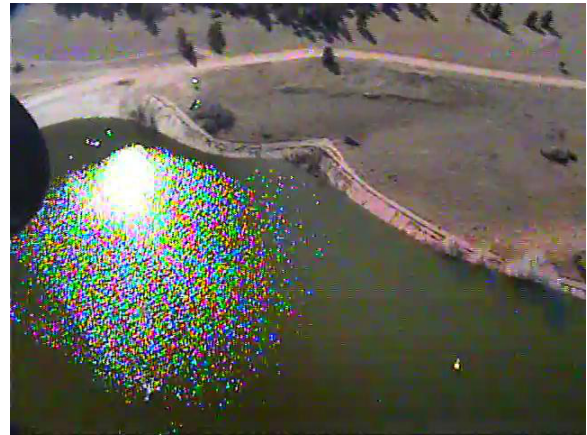

Fig. 1. An example image of sunlight reflection on water surfaces from one of our flight tests

Sparrow proposed a reflection model for a roughened surface consisting of v-shaped specular micro-facets [2]. Based on that assumption, they provided an analytical solution to explain off-peak light reflection. Addressing the problem from a real-time rendering perspective, Phong proposed a simple three-component model, consisting of ambient reflection, Lambertian diffuse reflection, and a specular component [3]. Oren and Nayar returned to the physical reflection models, further developing the approach of Torrance and Sparrow to model rough surfaces as v-shaped *Lambertian* micro-facets and computing an accurate off-plane reflection model [4]. In an extension of their work with Wolff, they included the effect of subsurface scattering to their model [5]. Sunlight glint from sea surfaces is dominated by reflection at the water surface. Cox and Munk emperically demonstrated that surface roughness is linearly correlated with wind speed [6].

Since realistic light-reflection models are important, we propose a variation on the Oren and Nayar's reflection model that includes both specular and diffuse components. The key contribution of our work is providing a mechanism for light-reflection avoidance to be incorporated into the UAV path planning process.

There is a significant body of literature on UAV path planning related to target detection/tracking. Due to space limitations, we restrict our review to a few closely-related works, focusing in particular on *local path planning* for *fixed-wing UAVs*. In our context, local path planning addresses path decisions made to effect the UAV's short term path, reserving the term global path planning (not covered here) with collection of multiple path planning steps. Dobrokhodov *et al.*

[1]H. Kwon, J. Yoder, S. Baek, and S. Gruber are with the Academy Center for UAS Research, Department of Electrical and Computer Engineering, United States Air Force Academy, USAFA, CO 80840, USA hyukseong.kwon@usafa.edu

[2]D. Pack is with the Department of Electrical and Computer Engineering, University of Texas, San Antonio, TX 78249, USA

suggested a small UAV system which is capable of detecting and tracking a mobile target on the ground with a gimbaled camera system [7]. In order to compensate for brief periods of lost detections, they used a linear parametrically varying (LPV) filter. Theodorakopoulos and Lacroix proposed a method using a lateral guidance law that adjusts the aircraft's roll angle to maintain a proper target view angle [8]. Quigley *et al.* designed a hierarchical UAV control system to perform multiple tasks: target detection, localization, and surveillance [9]. Their method dealt with flight path planning with high-level control and camera gimbaling with low-level control. Rafi *et al.* developed a single follow-and-orbit strategy and demonstrated in simulations that it kept a target vehicle in view in spite of the vehicle moving at different velocities while making turns in an urban environment [10]. Their work provided a circular flight path strategy considering target speed, UAV airspeed, and UAV maneuverability. Finally, Skoglar provided a good review of the UAV path planning literature in his thesis [11], as well as exploring several directions for UAV control and tracking of ground targets.

There is also more specific literature related to UAV path control considering no-fly zones. Among a number of publications, Bellingham *et al.* presented a receding horizon control to optimize a UAV's flight trajectory with no-fly zone constraints [12]. Their method solved a modified Mixed-Integer Linear Programming problem with two different functional levels of trajectory planning algorithms. Zengin and Dogan suggested a rule-based flight guidance strategy in the situation of mobile target pursuit [13]. Their method considered multiple factors of restricted region avoidance, target proximity maintenance, and threat exposure level minimization. In order to deal with multiple constraints, they used a probabilistic threat exposure map and a gradient search algorithm. Droge and Egerstedt proposed a solution to the problem of flying to a known target with unknown obstacles in the way [14]. In their paper, a UAV plans its current trajectory based on obstacles within its field of view, adaptively changing how far it looks ahead with its model-predictive control based on recent past performance of the various controllers.

Differently from the conventional methods mentioned in the above paragraph, we do not deal with 'no-fly' zones, but deal with 'non-preferred-fly' zones due to the sunlight reflected areas, which are the areas that we would like to avoid. Depending on location, date, time of day, the size and position of the area, passing through a non-preferred-fly zone could be the best decision. Our focus in this paper is to determine a UAV path or trajectory that minimizes the influence caused by sunlight-reflected background areas around a tracked target by finding a path that minimizes target detection uncertainty. Our novel approach proposes a UAV path planning method that avoids sunlight reflection around an estimated target location while maintaining appropriate UAV motion and target detection feasibility.

The remainder of the paper is organized as follows: Section II describes a relative geometry model with sun, target, sunlight reflection and UAV components. In this
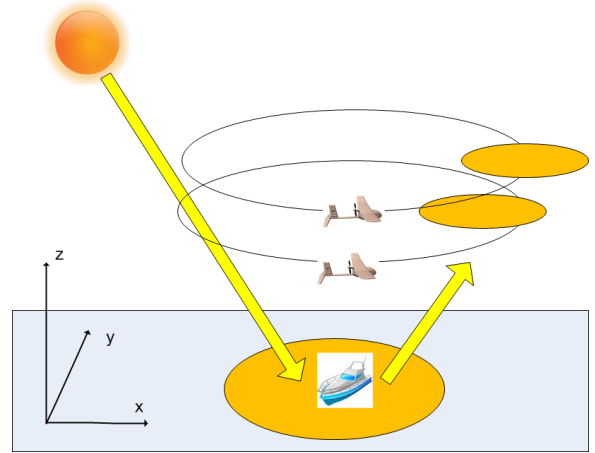

Fig. 2. Illustration of UAV motions related to sunlight reflection near a target location

section, the restricted UAV motion model effects on target detectability near sunlight reflection is described. Section III explains the setup of the sunlight reflection model that induces sunlight reflectance along UAV paths. Section IV proposes a technique for finding a preferable UAV path considering the sunlight reflection model, UAV motion, and uncertainty of estimated target location. Finally, simulation results validate our approach in Section V and Section VI concludes the paper.

II. UAV MOTION PREFERENCE WITH TARGET DETECTION

Throughout this paper, we define a *sunlight reflected area* as an area where a UAV cannot see the target due to sunlight reflection over the target location's area of uncertainty (see Fig. 2). Since the motion of a fixed-wing aircraft is nonholonomic, there are possible situations where the UAV needs to pass through target nonvisible areas due to sunlight reflection around the target location so that the UAV maintains an appropriate motion or distance to the target. In this section, we present how to define a UAV motion preference considering the UAV avionics and target detection using an image sensor for a fixed-wing UAV. In our proposed method, the UAV motion model assumes a constant velocity. Therefore, the UAV model can be simplified as,

$$\begin{bmatrix} \dot{x} \\ \dot{y} \\ \dot{\psi} \end{bmatrix} = \begin{bmatrix} v \cdot \sin(\psi) \\ v \cdot \cos(\psi) \\ \psi_{dev} \end{bmatrix} \qquad (1)$$

where x, y, and ψ are the UAV's x-coordinate value, y-coordinate value, and 'yaw' angle, respectively. And v is the tangential velocity of the UAV and ψ_{dev} is the yaw angle change from the previous estimation. The reference axis for ψ is the coordinate axis toward north (y-axis) in the world coordinate frame.

The basic target tracking approach used in this paper is shown in Fig. 2. While the UAV tracks a target on the water surface, a certain range of the UAV's path can be
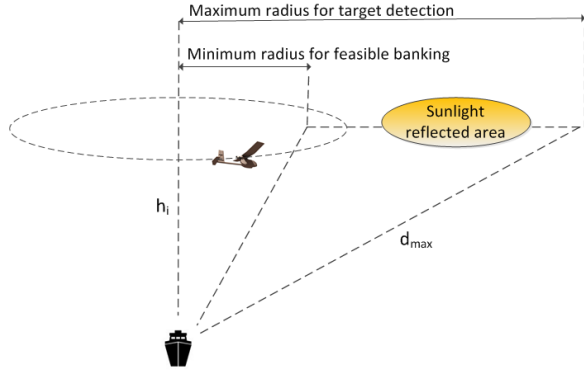
Fig. 3. Maximum and minimum UAV orbits at an altitude for target detectability

Fig. 4. Different UAV orbit candidates according to sunlight reflection ranges

affected by sunlight reflection. The camera sensor mounted on the UAV is affected by sunlight reflection from the water's surface near the target along a portion of each UAV orbit. As mentioned earlier, our goal is to find the UAV path around the estimated target location which minimizes the uncertainty of target localization.

Initially, the UAV persistently tracks the target, which means that the UAV tries to maintain a circular orbit around the target in order to have consistent target detection characteristics. As illustrated in Fig. 2, depending on UAV altitudes, the pattern of sunlight reflection for the same UAV orbit radius changes. Besides the UAV altitude, different orbit radii also provide different target detectability as shown in Fig. 3.

As depicted in Fig. 3, once a number of feasible altitude candidates are selected, the minimum and maximum orbit radii can be calculated for each altitude. The minimum radius is restricted by the maximum UAV bank angle. The minimum orbital radius r_{min} is calculated as

$$r_{min} = \frac{v^2}{g \cdot \tan \phi_{max}} \quad (2)$$

where g is the gravitational acceleration (9.8 m/s^2), and ϕ_{max} is the maximum UAV bank angle [15].

On the other hand, the maximum orbit radius r_{max} is determined by the maximum distance to detect a target with a designated sensor, which is an electro-optic sensor in our approach. With the maximally allowable distance-to-target as d_{max} (according to sensor capability), the maximum orbital radius r_{max} becomes

$$r_{max} = \sqrt{d_{max}^2 - h_i^2} \quad (3)$$

where h_i is the ith altitude candidate.

In our sensor system, target detectability is inversely proportional to the size of target localization uncertainty covariance. In order to compare two different covariance matrices, we use traces of covariances in this paper. Since the size of target localization uncertainty is proportional to the distance-to-target and the elevation angle-to-target, r_{min} with the lowest UAV altitude provides the best target detectability. However, if sunlight reflected areas are involved,
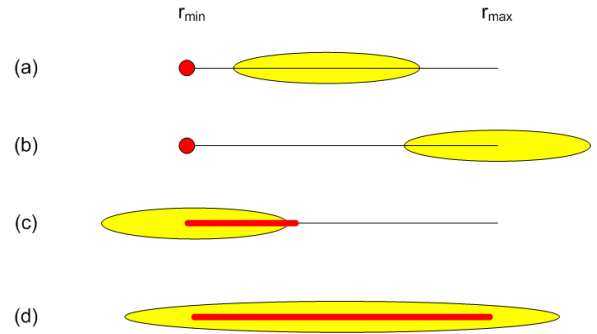
any candidate orbit could be the best one. Figure 4 presents four different cases where the target nonvisible area due to sunlight reflection can affect an orbital radius between r_{min} and r_{max}. In both of the cases shown in frames (a) and (b), the minimum orbital radius will be the best choice because it gives the best target detectability with no sunlight reflection influence. In the case shown in frame (c), we compare the orbital radius just outside sunlight reflected areas and other radii in the sunlight reflected areas. Finally in the case shown in frame (d), we must find an orbit radius with some minimal cost since sunlight reflection covers all possible UAV radii. Depending on the distribution of sunlight reflection, a certain path in the thick (red in colored prints) line becomes the best path in the cases shown in frames (c) and (d). In the following section, we explain how to determine the sunlight reflected area at each altitude along the UAV paths.

III. SUNLIGHT REFLECTION MODEL

In order to calculate accurate sunlight reflection affected areas according to target locations and relative UAV positions, we need to first calculate the amount of sunlight reflection. In our system, we assume that the weather condition is consistent. Therefore, when a UAV passes a sunlight reflected area, the sunlight reflected pattern has not changed until the UAV revisits the area.

Conceptually speaking, light reflection can be decomposed into various components: specular reflection, diffuse reflection, diffuse back-scatter, retroflection, and ambient components, to name a few. Since this paper deals with surface target perception from an image sensor mounted on a UAV, we simplify the light reflection model by using two major factors, specular reflection and directional diffuse reflection, as shown in Fig. 5.

The amount of directly reflected luminance depends on incident azimuth/elevation angles of sunlight rays to the water surface and reflected azimuth/elevation angles. Figure 6 illustrates a general light reflection with incident/reflected sunlight rays. In the figure, θ_i is the elevation angle of the incident light with respect to the surface normal, and ϕ_i is the corresponding azimuth angle with respect to any axis on the ground coordinate frame (e.g. the x-axis or y-axis). The reflected elevation and azimuth angles (θ_r and ϕ_r, resp.)
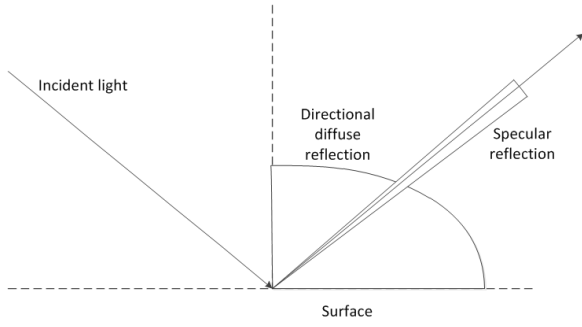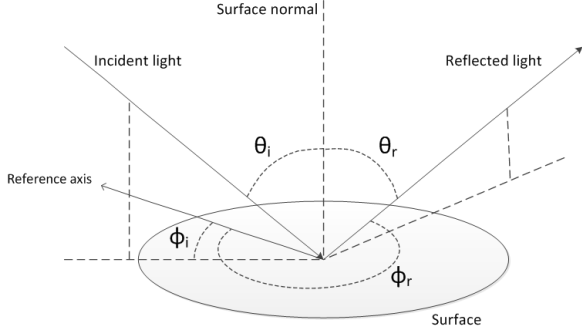
Fig. 5. Proposed sunlight reflection model

Fig. 6. Angles of incident/reflected light rays

Fig. 7. Sampling strategy of the proposed method

depend on the location of the UAV. Our model is based on Oren-Nayar's model [4], adjusted to include specularities. Equations 4 and 6 describe specular reflectance, L_r^S, and directional diffuse reflectance, L_r^D, respectively in our light reflection model.

$$L_r^S(\theta_r, \theta_i, \phi_r, \phi_i) = \frac{\rho}{\pi} L_i \cos\theta_i \cdot \delta_w(\theta_r - \theta_i, \phi_r - \phi_i - \pi) \quad (4)$$

where ρ is albedo, L_i is the incident sunlight strength, and $\delta_w(x,y)$ is a cylinder-like function with the following property.

$$\delta_w(\theta, \phi) = \begin{cases} 1, & \text{if } |\theta| < \theta_{th} \text{ and } |\phi| < \phi_{th} \\ 0, & \text{otherwise} \end{cases} \quad (5)$$

where θ_{th} is the threshold of elevation angular deviation and ϕ_{th} is the threshold of azimuth angular deviation between the incident light and the corresponding reflected light. If the angular deviation is larger than a certain threshold, we can consider that the view or target detection is not affected by the sunlight reflection. Although specular reflection is the most influential part, on an ideal flat water surface it affects a very narrow range of reflection angles. However, in practical cases, conditions such as roughness[1] of the water surface, make the affected region wider. The diffuse reflectance component, L_r^D, of our reflection model comes from [4], obtained through

---

[1]We assume that a rough estimate of the target's location is available, either from another sensing platform, or, in the case of tracking, from a previous observation.
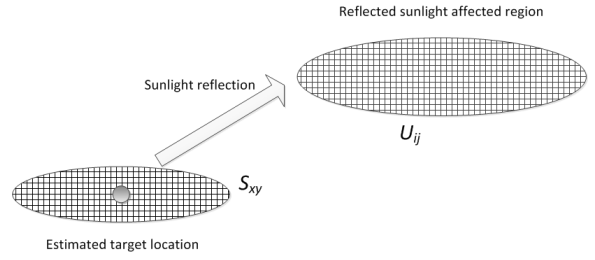
$$L_r^D(\theta_r, \theta_i, \phi_r, \phi_i) = \frac{\rho}{\pi} L_i \cos\theta_i \{C_1 + C_2 \sin\alpha \tan\beta$$
$$\cdot \max(0, \cos(\phi_r - \phi_i - \pi))\} \quad (6)$$

where

$$C_1 = 1 - 0.5\frac{\sigma^2}{\sigma^2 + 0.33}, \quad (7)$$

$$C_2 = 0.45\frac{\sigma^2}{\sigma^2 + 0.09}, \quad (8)$$

$$\alpha = \max(\theta_i, \theta_r), \quad (9)$$

and

$$\beta = \min(\theta_i, \theta_r). \quad (10)$$

where σ is the roughness of the surface. Finally, the total light reflectance, L_r, for each surface region with a certain perspective becomes,

$$L_r(\theta_r, \theta_i, \phi_r, \phi_i) = L_r^S(\theta_r, \theta_i, \phi_r, \phi_i) + L_r^D(\theta_r, \theta_i, \phi_r, \phi_i). \quad (11)$$

Based on the light reflection mentioned above, we can consider the following situation. Suppose that we have an estimated location of a target from another sensor platform, and that the UAV is approaching this location (or alternatively that the UAV is in the process of tracking the target).

To model the sunlight reflected area around the target's location on the water surface, we sample the sunlight reflected area on the water surface with $\mathbf{S} = \{S_{x,y}\}$ as shown in Fig. 7. And to plan the corresponding UAV's trajectory, we also sample the feasible area with $\mathbf{U} = \{U_{i,j}\}$. $\mathbf{U}$ contains expected sunlight reflected areas on the UAV's paths, which cover between r_{min} and r_{max}. Eventually, the search region is determined by a combination of feasible UAV paths, the estimated target location, and sun orientation. How to determine the UAV path candidates to avoid sunlight reflection was already described in Section II.

Finally, at each sampled cell, $U_{i,j}$, the predicted light reflectance L_{Ref} is calculated as,

$$L_{Ref}(U_{i,j}) = \sum_x \sum_y L_R(U_{i,j} \mid S_{x,y}) \quad (12)$$

where $L_{Ref}(U_{i,j} \mid S_{x,y})$ is light reflectance from $S_{x,y}$ to $U_{i,j}$.

As already represented in Fig. 1, if the target is in the area of full saturation of sunlight reflection or in a partially reflected area, it is difficult to detect small targets. Therefore,
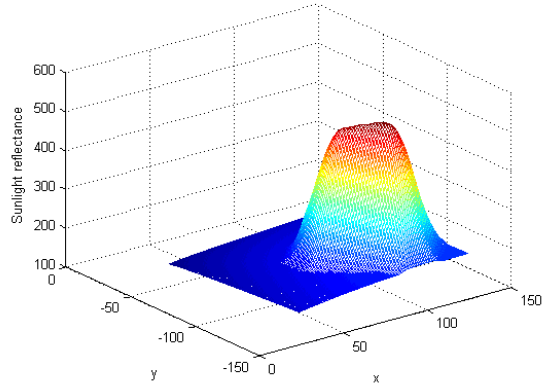
(a) Actual distribution
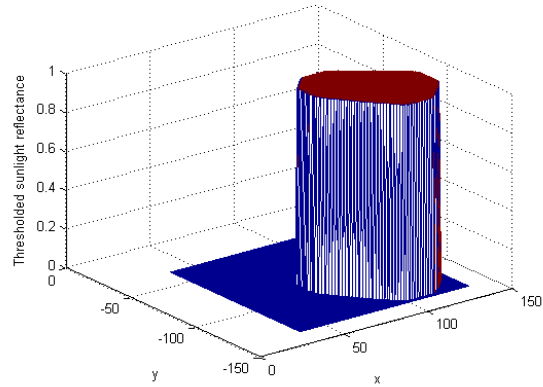
(b) Thresholded distribution

Fig. 8. Sunlight reflectance over the sampled area

if $L_{Ref}(U_{i,j})$ is more than a threshold (obtained from experiments and the corresponding image analysis), we consider $U_{i,j}$ as a "Target-Detection-Impossible-Section." Figure 8(a) shows a sample of sunlight reflectance distribution over the sample area, **U**, and Fig. 8(b) shows the corresponding thresholding from Fig. 8(a).

IV. INTEGRATED UAV PATH PLANNING

By using information defined in Section II and Section III, we can define the best UAV path to minimize target localization uncertainty. First, we define the target localization uncertainty. When the UAV's sensor has a target in its field of view, the UAV can localize the target with localization uncertainty as shown in Fig. 9. The uncertainty σ in the sensor view induces the uncertainty Σ around the target on the water surface.

If we set uncertainty in the sensor view as a circle with radius σ, the uncertainty Σ becomes an ellipse. We define the length of the major axis of the ellipse as λ_{max}, that of the minor axis as λ_{min}, the corresponding eigenvector to λ_{max} as $\vec{v}_{max}$, and the corresponding eigenvector to λ_{min} as $\vec{v}_{min}$. Then, the covariance matrix Σ will be
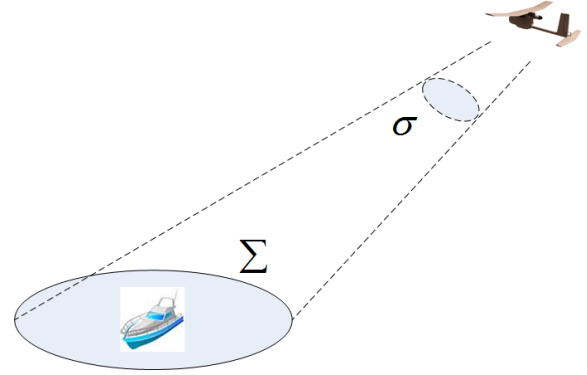

Fig. 9. Target localization uncertainty

$$\Sigma = V \begin{bmatrix} \lambda_{max} & 0 \\ 0 & \lambda_{min} \end{bmatrix} V^T \qquad (13)$$

where $V = \begin{bmatrix} \vec{v}_{max} & \vec{v}_{min} \end{bmatrix}$.

After we initialize the uncertainty Σ, each additional observation generates a measurement uncertainty Σ_{meas} for the same target with the same approach. Then the updated uncertainty $\Sigma_{updated}$ becomes

$$\Sigma_{updated} = \left[\Sigma^{-1} + \Sigma_{meas}^{-1} \right]^{-1} \qquad (14)$$

Or due to sunlight reflection, if the UAV loses track of a target, the uncertainty increases with target motion uncertainty value λ_t.

$$\Sigma_{updated} = V \begin{bmatrix} \lambda_{max} + \lambda_t & 0 \\ 0 & \lambda_{min} + \lambda_t \end{bmatrix} V^T \qquad (15)$$

Along the selected paths shown in Section II, we calculate cumulative covariance changes. Then we select the path which indicates the smallest peak covariance or the smallest average covariance. If the mission goal is to limit the covariance as much as possible, we choose the smallest peak covariance. On the other hand, if the mission goal is to have a more accurate target localization on average during the whole orbit, the smallest average covariance should be considered.

The summary of the proposed method is shown in Algorithm 1.

V. SIMULATION RESULTS

In this simulation to track a stationary target, we used the following realistic parameters:

- Target location: 37°23'35.63"N, 124°15'34.57"W (Near San Francisco Bay)
- UAV altitude: 125 – 175 m
- UAV velocity: 20 m/s
- UAV maximum bank angle: 18°
- Sensor frame rate: 5 frames/sec
- Date: March 15, 2013

With the attitude choices of 125 m, 150 m, and 175 m above sea level, and the time around 12:00 PM (azimuth of sun is 173.12 degrees and its elevation is 50.21 degrees),

Algorithm 1 Proposed algorithm

Determine **S** around the estimated target location.
Determine candidates of feasible UAV altitudes.
for each UAV altitude
      Find r_{min} and r_{max}.
      Determine the sunlight reflection area **U**.
end
for each x,y
      Estimate $L_R(U_{x,y})$.
end
Threshold $L_R(U_{x,y})$.
for each UAV altitude
      for each UAV path
            Estimate Σ's along each UAV path.
   end
end
Choose the optimal UAV path.

the path candidates are shown in Fig. 10(a) through (c). The circular contours are UAV path candidates and irregular contours (in magenta in colored prints) are the sunlight reflected areas. Solid line paths (in blue in colored prints) are non-optimal UAV paths, and the path with ∘-symbols (in red in colored prints) is the optimal path chosen with the proposed criteria. The locations of the ∘-symbols show the point where the image is taken.

In order to depict the change of sunlight reflection and its related UAV path change, Figures 11 through 14 show simulation results for different times. Figure 11(a) shows a three dimensional visualization of the UAV path candidates with the corresponding sunlight reflection areas. The path with ∘-symbols is the optimal path which is chosen when it is 10:00 AM (azimuth: 133.22°, elevation: 39.21°). Fig. 11(b) shows a comparison of covariance changes for each UAV path. For a better view of the covariance changes, each value is shown as the log-value of the traces of covariance matrices. The thick solid line (in red in colored prints) shows the optimal candidate and the dashed lines show other candidates. Fig. 12, Fig. 13, and Fig. 14 show results at 12:00 PM (azimuth: 173.12°, elevation: 50.21°), 2:00 PM (azimuth: 216.83°, elevation: 43.91°), and 4:00 PM (azimuth: 245.83°, elevation: 25.33°), respectively. Readers can see that the higher elevation of the sun provides the wider sunlight reflected area near the estimated target location, which results in the more complicated path selection.

TABLEs I through IV show quantified results of the number of frames that lost track of the target, the average distance-to-target, the average elevation angle to the target from the UAV, and the maximum trace of covariance in relation to the UAV's altitude and orbital radius. The candidates marked with ∗ show the optimal choice with the smallest maximum trace of covariance (bold fonts).
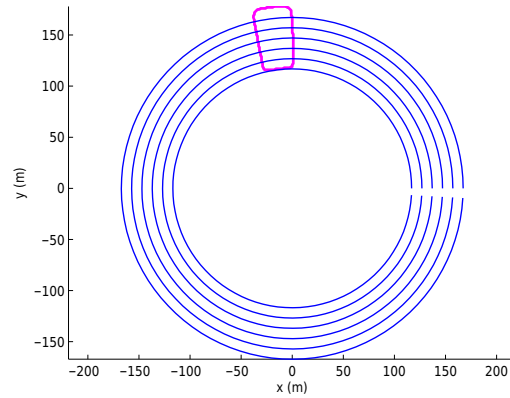
VI. CONCLUSION

In this paper, we presented an approach for UAV path planning that maximizes target detection feasibility while
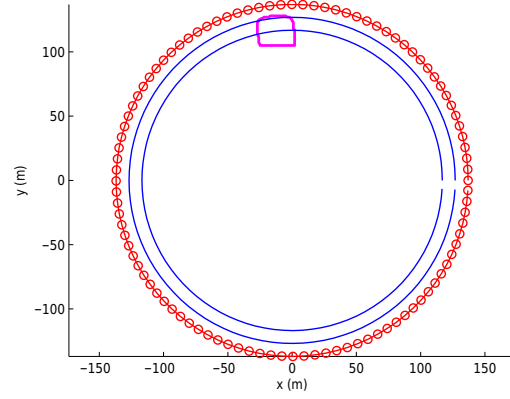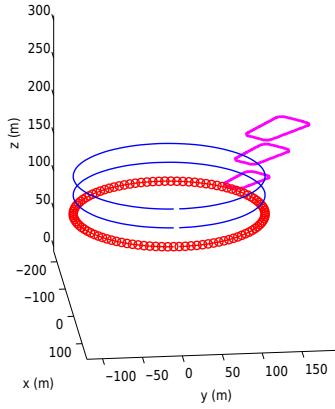

(a) At 125 m altitude
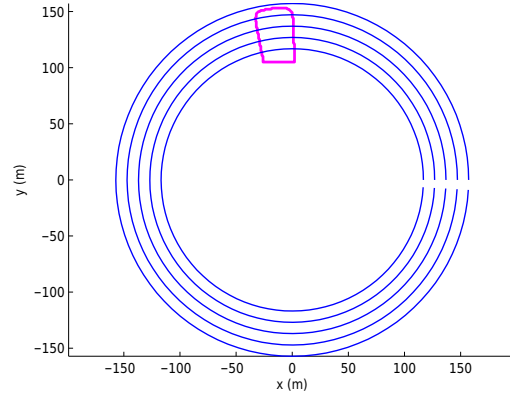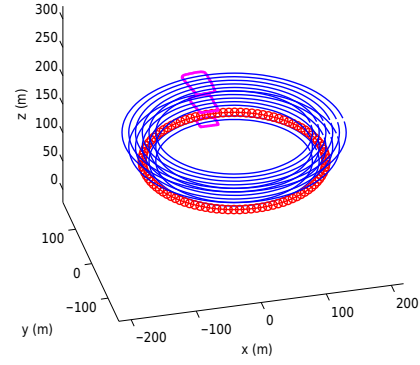

(b) At 150 m altitude

(c) At 175 m altitude

Fig. 10. UAV path candidates for each altitude at 12:00PM

TABLE I
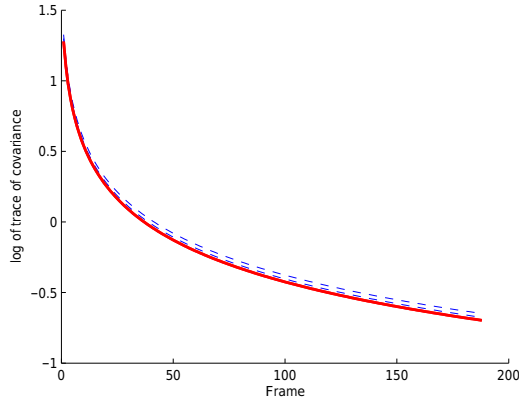
SIMULATION TEST RESULT FOR 10:00AM

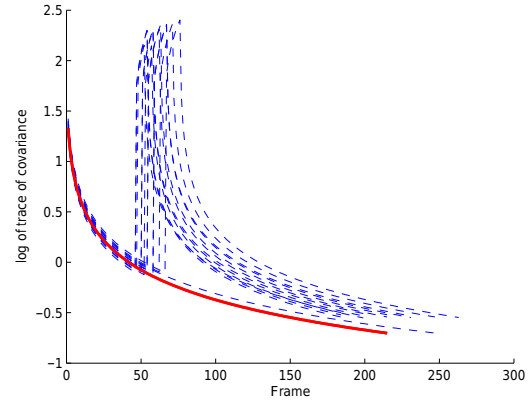| Altitude (m)	Orbital radius (m)	Target loss (frames)	Distance to target (m)	Elevation to target (°)	Maximum trace of covariance
*125.0	119.6	0	173.0	46.28	**18.99**
150.0	119.6	0	191.8	51.44	19.92
175.0	119.6	0	211.9	55.66	21.21

(a) UAV paths

(b) Covariances over time

Fig. 11.   Result for time 10:00AM

(a) UAV paths

(b) Covariances over time

Fig. 12.   Result for time 12:00PM

TABLE II

SIMULATION TEST RESULT FOR 12:00PM

Altitude (m)	Orbital radius (m)	Target loss (frames)	Distance to target (m)	Elevation to target (°)	Maximum trace of covariance
125.0	116.8	8	171.1	46.93	197.28
125.0	126.8	5	178.1	44.57	139.95
*125.0	136.9	0	185.4	42.39	**21.41**
150.0	116.8	8	190.1	52.08	199.26
150.0	126.8	8	196.4	49.77	201.50
150.0	136.9	8	203.1	47.60	203.91
150.0	147.1	9	210.0	45.55	226.54
150.0	157.1	0	217.2	43.66	24.65
175.0	116.8	5	210.4	56.27	141.91
175.0	126.8	8	216.1	54.05	203.85
175.0	136.9	9	222.2	51.95	225.94
175.0	147.1	9	228.6	49.94	228.20
175.0	157.1	9	235.2	48.07	230.59
175.0	167.2	10	242.0	46.30	253.13

TABLE III

SIMULATION TEST RESULT FOR 2:00PM

Altitude (m)	Orbital radius (m)	Target loss (frames)	Distance to target (m)	Elevation to target (°)	Maximum trace of covariance
125.0	120.0	7	173.2	46.16	178.10
125.0	132.2	7	181.9	43.39	181.44
125.0	145.0	8	191.4	40.76	205.29
125.0	157.2	6	200.8	38.49	169.29
125.0	170.0	0	211.0	36.32	26.91
*150.0	120.0	0	192.0	51.34	**19.97**
175.0	120.0	0	212.1	55.56	21.25

TABLE IV

SIMULATION TEST RESULT FOR 4:00PM

Altitude (m)	Orbital radius (m)	Target loss (frames)	Distance to target (m)	Elevation to target (°)	Maximum trace of covariance
*125.0	119.5	0	172.9	46.28	**18.99**
150.0	119.5	0	191.8	51.45	19.92
175.0	119.5	0	211.9	55.67	21.21

minimizing sunlight reflection. In order to estimate sunlight reflection, we used our customized light reflection model containing specular and directional diffuse reflectances and sampled sunlight reflected regions near the estimated target location and the corresponding areas along UAV paths. In order to find the best UAV path, we estimated target lo-
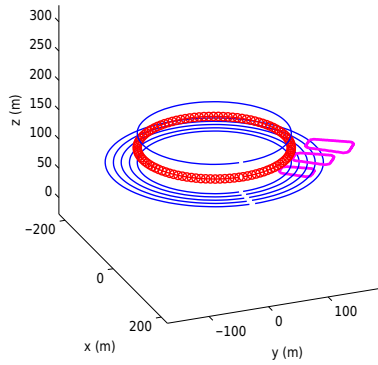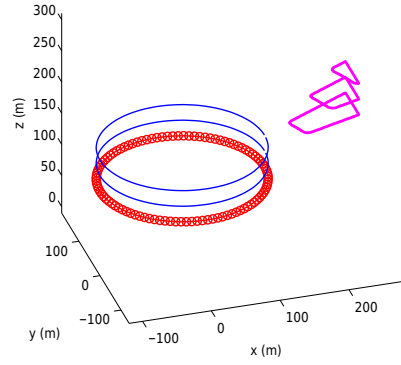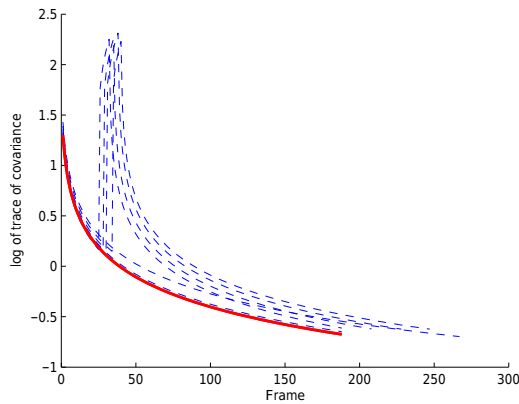
calization uncertainty covariances along feasible UAV paths considering target detectability. We then found the path which presented the smallest peak covariance or average
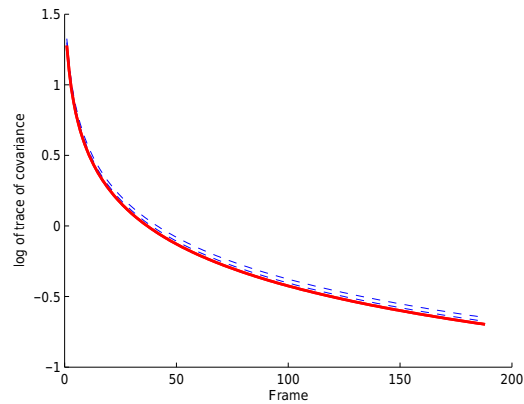
(a) UAV paths

(b) Covariances over time

Fig. 13. Result for time 2:00PM

(a) UAV paths

(b) Covariances over time

Fig. 14. Result for time 4:00PM

covariance, depending on the mission requirement. Simulation tests validated our approach. Future work includes a path planning approach with mobile target tracking and a sunlight reflected area compensation using computer vision techniques.

ACKNOWLEGEMENT

We would like to thank Dr. Rajnikant Sharma of the U.S. Air Force Academy/University of Texas in San Antonio for his helpful inputs and discussions.

REFERENCES

[1] N. Fred, "Directional Reflectance and Emissivity of an Opaque Surface," Applied Optics, vol. 4, no. 7, pp. 767–775, 1965.
[2] K. E. Torrance and E. M. Sparrow, "Theory of Off-Specular Reflection from Roughened Surfaces," Journal of the Optical Society of America, vol. 57, no. 9, pp. 1105–1114, 1967.
[3] B. T. Phong, "Illumination for Computer Generated Pictures," Communications of ACM, vol. 18, no. 6, pp. 311–317, 1975.
[4] M. Oren and S. K. Nayar, "Generalization of Lambert's Reflectance Model" SIGGRAPH, July, 1994.
[5] L. B. Wolff, M. Oren and S. K. Nayar, "Improved Diffuse Reflection Models for Computer Vision," International Journal of Computer Vision, Vol. 30, no. 1, pp. 55–71, 1998.
[6] C. Cox and W. Munk, "Measurement of the Roughness of the Sea Surface from Photographs of the Sun's Glitter," Journal of the Optical Society of America, vol. 44, no. 11, pp. 838–850, 1954.
[7] V. N. Dobrokhodov, I. I. Kaminer, K. D. Jones and R. Ghabcheloo, "Vision-Based Tracking and Motion Estimation for Moving targets using Small UAVs," Proc. of the 2006 American Control Conference, June, 2006.
[8] P. Theodorakopoulos and S. Lacroix, "A Strategy for Tracking a Ground Target with a UAV," Proc. of IEEE Intelligent Robots and Systems, 2008.
[9] M. Quigley, S. Griffiths, and R. W. Beard, "Target Acquisition, Localization, and Surveillance using a Fixed-Wing Mini-UAV and Gimbaled Camera," Proc. of IEEE International Conference on Robotics and Automation, 2005.
[10] F. Rafi, S. Khan, K. Shafiq and M. Shah, "Autonomous Target Following by Unmanned Aerial Vehicles," SPIE Defense and Security Symposium, 2006.
[11] P. Skoglar, "Planning Methods for Aerial Exploration and Ground Target Tracking," Ph.D. Thesis, Linkoping University, 2009.
[12] J. Bellingham, A. Richards, and J. P. How, "Receding Horizon Control of Autonomous Aerial Vehicles," Proc. of American Control Conference, 2002.
[13] U. Zengin and A. Dogan, "Real-Time Target Tracking for Autonomous UAVs in Adversarial Environments: A Gradient Search Algorithm," IEEE Transactions on Robotics, Vol. 23, No. 2, pp.294–307, 2007.
[14] G. Droge and M. Egerstedt, "Adaptive Look-Ahead for Robotic Navigation in Unknown Environments," Proc. of IEEE/RSJ International Conference on Intelligent Robots and Systems, 2011.
[15] L. J. Clancy, "Aerodynamics," Pitman Publishing Limited, London, 1975.